Eurographics Conference on Visualization (EuroVis) 2014
H. Carr, P. Rheingans, and H. Schumann
(Guest Editors)

Volume 33 (2014), Number 3

Vortex Detection in 4D MRI Data: Using the Proper Orthogonal Decomposition for Improved Noise-Robustness

Robert Carnecky[1], Thomas Brunner[1], Silvia Born[2], Jürgen Waser[3], Christian Heine[1], Ronald Peikert[1]

[1]ETH Zurich, Switzerland
[2]University of Zurich, Switzerland
[3]VRVis Vienna, Austria

Abstract

Recent advances in magnetic resonance imaging (MRI) technology enabled the acquisition of time-resolved 3D blood flow data. Several flow visualization methods have been applied to these data in order to investigate links between cardiovascular diseases and hemodynamic phenomena, such as vortices in the blood flow. In this work, we investigate the use of the proper orthogonal decomposition (POD) for the preprocessing of MRI datasets and study its effects with the λ_2 vortex detection method. By comparing the POD method with the commonly used Gaussian filtering, we show that for comparable filtering strengths, the POD produces qualitatively better results.

1. Introduction

In a healthy cardiovascular system, morphology and hemodynamics are attuned to one another. The specific geometry of the heart and vessels allows an efficient blood circulation through the body. The blood flow exerts mechanical forces on the vessel walls and triggers a continuous renewal of the tissue. However, if either morphology or hemodynamics develop anomalies, their synchronized interplay gets out of balance and cardiovascular diseases may develop [RE06].

In this process of disease development, vortices play an important role. Vortices are not per se an indicator for a cardiovascular dysfunction since healthy blood flow also comprises recirculation and vortices — especially in curved regions or at bifurcations [KYM*93, Dav95]. Still, vortices often occur abnormally because of morphological alterations, e.g., in vessel widenings or after narrowings (stenosis, calcified heart valves). In these cases, the vortical flow alters the pressure and shear forces on the vessel walls (in direction, frequency, or magnitude) and triggers cellular processes leading to aneurysms or atherosclerosis [Dav95]. Also, in slowly rotating vortices the thrombogenesis risk is increased, since the blood may come to a halt and start to clot. These thrombi can cause stroke or heart attacks [FAH*08].

Altogether, pathologies are indicated when vortices appear in unusual regions, persist exceptionally long, or show very low blood velocities. Therefore, a strong research interest exists in the more detailed relationship between vortical flow and specific diseases and their progression [FAH*08]. For this, vortices are examined in 4D MRI blood flow data. 4D MRI is a flow-sensitive imaging technique, which allows to measure time-resolved blood flow velocities in three dimensions. In these data, automatic vortex detection has so far been done with algorithms commonly used with simulation data [SFH*10, BPM*13, KGP*13]. However, the results are not satisfactory yet because 4D MRI has lower resolution and signal-to-noise ratio as well as different noise characteristics than simulation data. Since the vortex detection algorithms rely on first- and second-order derivatives, they are especially sensitive to lower-quality flow data like 4D MRI.

Our approach is therefore to preprocess the 4D MRI data to improve vortex detection. In particular, we propose the use of the proper orthogonal decomposition (POD), which decomposes the velocity field into different scales of motion. Its use is motivated by the fact that vortices in blood flow are medium- to large-scale phenomena, while noise is a small-scale phenomenon. By discarding the high-frequency scales, we seek to improve the quality of the detected vortices.

2. Related Work

Although a *vortex* is an intuitive flow phenomenon, it has no unique mathematical definition. In a recent work, Köhler et al. compare existing vortex extraction methods for 4D MRI data, identifying the λ_2 method as the most appropriate [KGP*13].

Based on the principal component analysis, *proper orthogonal decomposition* (POD) [Lum67] is a decomposition of a velocity field into its different scales of motion, which is an established method especially in turbulence research. Pobitzer et al. [PTA*11] examine POD in combination with feature extraction from time-dependent velocity fields. McGregor et al. [MSS*08] apply POD to simulated blood flow in order to obtain a basis model of the flow, which is used to enhance measured data.

A wide range of *flow visualization* methods have been applied to blood flow data. Integration-based visualization is used, e.g., in the Quantitative Flow Explorer framework by van Pelt et al. [vPOBB*10] for interactive exploration of 4D MRI data. Standard flow visualization techniques, when applied to MRI data, often suffer from noisy data. Friman et al. [FHH*10] estimate the noise parameters from 4D MRI data and visualize uncertain streamlines. A different approach to cope with noise is the use of pathline predicates [SGSM08]. This technique has been used by Born et al. for a framework where the user can filter relevant integral lines [BPMS12], and by Köhler et al. [KGP*13] for visualization of vortices extracted from 4D MRI data. Recently, illustrative flow visualization techniques [BCP*12] have found their way into blood flow visualization. Born et al. improve the expressiveness of their visualizations by applying illustrative rendering to representative line bundles [BMGS13].

3. 4D MRI

"4D PC-MRI" is a technical name for time-resolved three dimensional phase-contrast magnetic resonance imaging, which is a method capable of acquiring a time-dependent vector field of a patient's blood flow [MFK*12]. In general, a 4D PC-MRI dataset consists of several time steps spanning a single heart beat, where each time step contains one magnitude and three phase difference images (see Fig. 1).

Due to the nature of MRI measurements, the resulting blood flow data contains a high amount of noise and inaccuracies [WKM08]. Partly, these are systematic errors, which can be corrected by specialized preprocessing methods [MKS*97, LHM*05, LTMG13]. Additionally, datasets contain noise. Noise in the raw measurements is often modeled as independent Gaussian noise. Since MRI acquires complex-valued frequency space raw data, noise in the resulting magnitude and phase offset images follow complicated distributions, which, however, can be approximated by Gaussian distributions if the signal-to-noise ratio (SNR) is high enough [GP95].

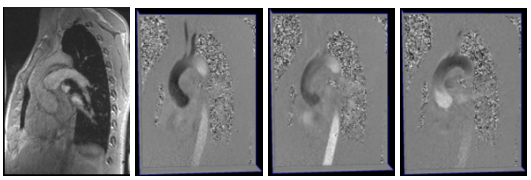

Figure 1: *A slice of a 4D MRI dataset with (from left to right) magnitude channel and u,v and w velocities.*

Apart from generic image processing algorithms, specialized methods have been proposed for the denoising of magnitude images, focusing on the reconstruction of anatomical features and often considering the Rician distribution of the noise [MCC*13]. In flow fields, noise can be reduced by imposing a divergence-free condition inside the blood vessel [BGWK13] or comparing measured data with a database of numerically simulated datasets [MSS*08]. Unlike these methods, our approach does not require a precise segmentation of the vessel or any a-priori knowledge about the data.

4. Proper Orthogonal Decomposition

The proper orthogonal decomposition (POD) [Loe63] approximates each of N outcomes $S^{(n)}(\mathbf{x})$ of a random scalar field variable by a "best fit" linear combination of $M \leq N$ uncorrelated *modes* $\hat{S}_i$. The n^{th} field is approximated

$$\hat{S}^{(n)}(\mathbf{x}) = \hat{S}_0(\mathbf{x}) + \sum_{i=1}^{M} a_i^{(n)} \hat{S}_i(\mathbf{x}), \qquad (1)$$

where $\hat{S}_0(\mathbf{x})$ is the mean of all outcomes and $\hat{S}_i$ are eigenfunctions to the M largest eigenvalues of the two-point spatial correlation operator [Loe63]. Because random noise has a low spatial correlation, it tends to reside in modes of low eigenvalues. Hence, if $M < N$, POD removes noise.

Lumley [Lum67] extended POD from scalar fields to vector fields and showed that the modes decompose a vector field into large-scale and small-scale phenomena. Sirovich [Sir87] proposed what is now known as snapshot POD. The N outcomes are simply taken to be snapshots of a time-dependent vector field at different times, therefore the approximations give a new time-dependent field.

Since there is no noise-free ground truth for 4D MRI, we tested the noise suppression capability of POD on synthetic data of a circular flow in a torus. The flow varies over time only by a factor and thus contains a single POD mode. A constant amount of white noise has been added to all (17) time steps, see Fig. 2. While in the full data, the noise accounts for 65.9% of the total energy, this is reduced to 10.2% if data are reconstructed from a single POD mode.

5. Results

In this section, we compare the POD method with simple Gaussian smoothing for the visualization of vortices in aortic blood flow. In accordance with the findings of Köhler et al. [KGP*13], we have chosen the λ_2 method [JH94] for extracting vortices from 4D MRI data. Note that Pobitzer et al. argue that the POD is incompatible with the λ_2 method

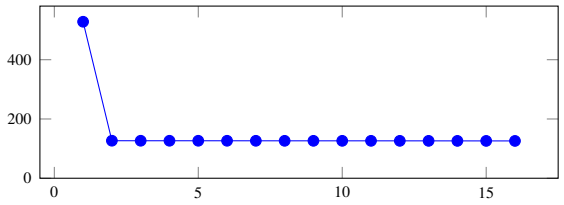

Figure 2: *Singular values (proportional to the square root of the energy) in POD of synthetic data, plotted per mode.*

since POD extracts large-scale features, whereas λ_2 is related to small-scale features [PTA*11]. In our application however, we are interested in large-scale vortices. Disjoint vortex core regions are obtained by using negative isosurface levels [JHSK97, DD00]. Both methods were implemented in the Visdom visualization framework [WFR*10].

All tests are performed on one of the following three datasets: a healthy aorta from a volunteer (Fig. 3(a)), a dataset with an aneurysm in the descending aorta (Fig. 3(b)), and an aorta with a pathologically distorted shape (Fig. 3(c)). The datasets have a spatial resolution of $192 \times 144 \times 26$ voxels, a temporal resolution of 17 to 22 time steps, and are preprocessed as described in [BFS*10, MHB*07].

(a) Healthy (b) Aneurysm (c) Distorted

Figure 3: *Approximate segmentations of datasets, computed as isosurfaces of the PCMRA field [BFS*10]. Models were manually cleaned to improve visual quality.*

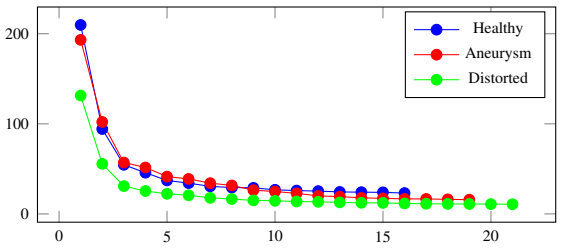

Figure 4: *Spectrum of singular values in the POD. The horizontal axis shows the index of the mode.*

Fig. 4 shows the spectrum of singular values when applying POD to our datasets. The energy of the modes decays fast, but does not reach zero. Note that a white noise random vector field has a perfectly flat spectrum. It is therefore likely that the first few modes have high SNR, while the last few modes contain mostly noise. Because the noise is distributed among all modes, the POD-filtered data will still be slightly noisy, even if using a very low number of modes. A way to further reduce noise is to do gradient estimation using a Gaussian derivative kernel instead of finite differences.

Gaussian smoothing and the POD are fundamentally different methods. However, they both have one parameter (σ and the number of modes, respectively) which controls the strength of the filtering effect. In order to select comparable values of these parameters, we compute the amount of change introduced to the original data by

$$\text{change}(t) = \sqrt{\sum_i \|\hat{\mathbf{v}}(\mathbf{x}_i,t) - \mathbf{v}(\mathbf{x}_i,t)\|_2^2}, \qquad (2)$$

where $\hat{\mathbf{v}}(\mathbf{x},t)$ is the filtered and $\mathbf{v}(\mathbf{x},t)$ the original vector field. Given two filtered datasets with comparable change(t), we can now do a qualitative comparison of detected vortices.

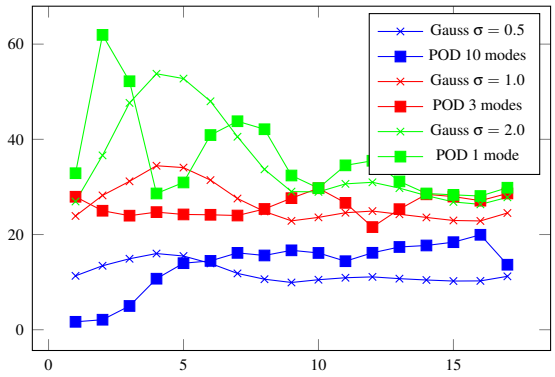

Figure 5: *Change in the healthy aorta dataset introduced by filtering methods.* change(t) *is plotted against the time step.*

Fig. 6 shows the detected vortices in the healthy aorta dataset. Filtering methods were performed on the original dataset, but the resulting λ_2 isosurfaces were clipped to only include the relevant part of the aorta. Depicted in yellow is the isosurface of the PCMRA field [BFS*10], showing an approximate static segmentation of the aorta for context purposes. The number of modes was chosen subjectively after inspecting the spectrum of singular values (Fig. 4). The corresponding value of σ for the Gaussian filtering was chosen such that both methods modify the original data approximately by the same amount (Fig. 5). Fig. 6 shows several combinations of preprocessing methods (POD and Gaussian filtering) and methods for computing derivatives (finite differences and convolution with Gaussian derivatives). Further results are shown in the accompanying video.

The time step chosen for Fig. 6 is at the end of the diastole, where the blood flows slowly and the SNR is small. Medical

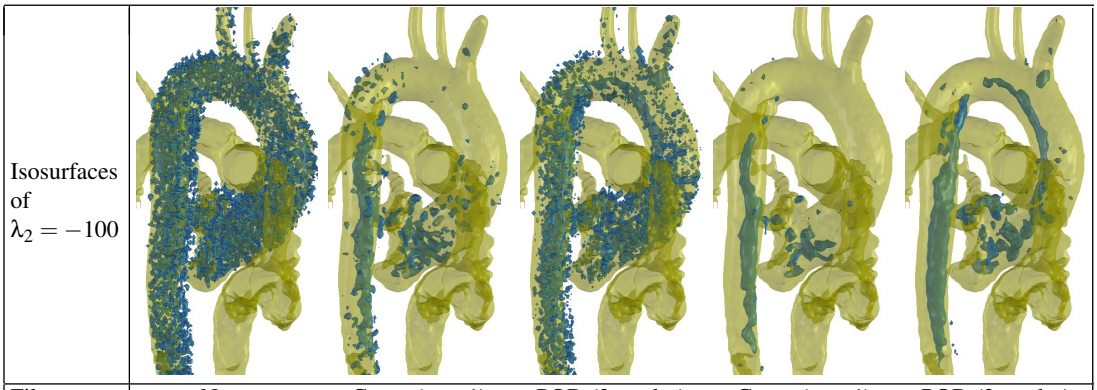

Figure 6: *Comparison of filtering methods for the healthy aorta dataset at the end of the diastole.*

literature tells us that the blood forms rotational flow patterns at this time (see Fig. 7), which is consistent with the tube-like structures of the λ_2 isosurfaces. Note that naïvely using finite differences without any preprocessing does not produce useful results. A POD reconstruction with 3 modes shows considerably less noise and vortical structures start to become visible. In comparison, Gaussian filtering yields smoother results at the cost of finding fewer features. After using Gaussian derivatives, results are comparable in visual quality, while the POD method shows more features. In order to verify that features visible in the POD-processed dataset correspond to a vortical flow, we seed streamlines of the original dataset around the features (Fig. 8).

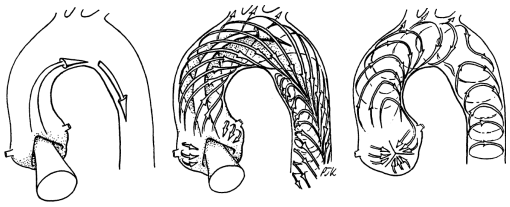

Figure 7: *Illustrative visualization of the blood flow in the aorta. (a) Early systole, accelerating axial flow. (b) Mid systole, secondary helical flows develop. (c) Late systole, rotational and recirculating secondary flows. Image reprinted with permission from [KYM*93].*

6. Conclusion

We have analyzed the use of the POD method for the preprocessing of PC-MRI blood flow dataset and its effect on the detection of vortices using the λ_2 method. Our results show that data processed with the POD method yields better results than the unprocessed data. A simple Gaussian filtering

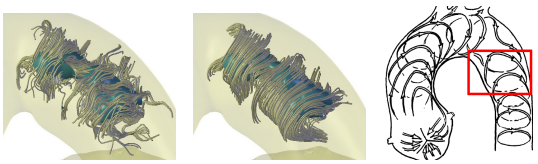

Figure 8: *Streamlines around features found in the POD-filtered distorted aorta dataset, showing that those are not false positives. (a) Streamlines in the original dataset. (b) Streamlines after Gaussian smoothing with $\sigma = 1$. (c) Corresponding region with expected helical flow.*

with the same filtering strength as POD produced smoother results, but resulted in fewer vortices being detected. As some amount of noise is contained in all POD modes, the standard gradient estimation based on finite differences does not produce sufficiently smooth results. By using instead a Gaussian derivative kernel, we achieved good results.

As there is no ground truth for measured MRI data, we did not perform a rigorous quantitative analysis of the POD method. Such an analysis could be performed on numerically simulated data with a physically correct model for PC-MRI noise, which is an interesting topic for future work.

Acknowledgments

The authors would like to thank Prof. Michael Markl for the MRI datasets. This work was funded by the Swiss National Science Foundation under grant 200021_127022, the ETH grant 12 09-3, and the Future and Emerging Technologies (FET) program of the European Commission, under FET-Open grant number 226042.

References

[BCP*12] BRAMBILLA A., CARNECKY R., PEIKERT R., VIOLA I., HAUSER H.: Illustrative Flow Visualization: State of the Art, Trends and Challenges. In *EG 2012 - State of the Art Reports* (2012), Eurographics Association, pp. 75–94. 2

[BFS*10] BOCK J., FRYDRYCHOWICZ A., STALDER A. F., BLEY T. A., BURKHARDT H., HENNIG J., MARKL M.: 4D phase contrast MRI at 3T: Effect of standard and blood-pool contrast agents on SNR, PC-MRA, and blood flow visualization. *Magn. Reson. Med. 63*, 2 (2010), 330–338. 3

[BGWK13] BUSCH J., GIESE D., WISSMANN L., KOZERKE S.: Reconstruction of divergence-free velocity fields from cine 3d phase-contrast flow measurements. *Magn. Reson. Med. 69*, 1 (2013), 200–210. 2

[BMGS13] BORN S., MARKL M., GUTBERLET M., SCHEUERMANN G.: Illustrative Visualization of Cardiac and Aortic Blood Flow from 4D MRI Data. In *Proc. IEEE PacificVis* (2013), pp. 129–136. 2

[BPM*13] BORN S., PFEIFLE M., MARKL M., GUTBERLET M., SCHEUERMANN G.: Visual Analysis of Cardiac 4D MRI Blood Flow Using Line Predicates. *IEEE Trans. Vis. Comput. Graph. 19*, 6 (2013), 1–14. 1

[BPMS12] BORN S., PFEIFLE M., MARKL M., SCHEUERMANN G.: Visual 4D MRI blood flow analysis with line predicates. In *Proc. IEEE PacificVis* (2012), pp. 105–112. 2

[Dav95] DAVIES P. F.: Flow-Mediated Endothelial Mechanotransduction. *Physiol. Rev. 75*, 3 (1995), 519–560. 1

[DD00] DUBIEF Y., DELCAYRE F.: On coherent-vortex identification in turbulence. *Journal of Turbulence 1* (2000), N11. 3

[FAH*08] FRYDRYCHOWICZ A., ARNOLD R., HIRTLER D., SCHLENSAK C., STALDER A. F., HENNIG J., LANGER M., MARKL M.: Multidirectional Flow Analysis by Cardiovascular Magnetic Resonance in Aneurysm Development Following Repair of Aortic Coarctation. *J. Cardiovasc. Magn. Res. 10*, 30 (2008). 1

[FHH*10] FRIMAN O., HENNEMUTH A., HARLOFF A., BOCK J., MARKL M., PEITGEN H.-O.: Probabilistic 4D Blood Flow Mapping. In *Medical Image Computing and Computer-Assisted Intervention – MICCAI 2010*. Springer, 2010, pp. 416–423. 2

[GP95] GUDBJARTSSON H., PATZ S.: The Rician Distribution of Noisy MRI Data. *Magn. Reson. Med. 34*, 6 (1995), 910–914. 2

[JH94] JEONG J., HUSSAIN F.: On the identification of a vortex. *J. Fluid. Mech. 285* (1994), 69–94. 3

[JHSK97] JEONG J., HUSSAIN J., SCHOPPA W., KIM J.: Coherent structures near the wall in a turbulent channel flow. *J. Fluid Mech. 332* (1997), 185–214. 3

[KGP*13] KÖHLER B., GASTEIGER R., PREIM U., THEISEL H., GUTBERLET M., PREIM B.: Semi-Automatic Vortex Extraction in 4D PC-MRI Cardiac Blood Flow Data using Line Predicates. *IEEE Trans. Vis. Comput. Graph. 19*, 12 (2013), 2773–2782. 1, 2, 3

[KYM*93] KILNER P. J., YANG G. Z., MOHIADDIN R. H., FIRMIN D. N., LONGMORE D. B.: Helical and Retrograde Secondary Flow Patterns in the Aortic Arch Studied by Three-Directional Magnetic Resonance Velocity Mapping. *Circulation 88* (1993), 2235–2247. 1, 4

[LHM*05] LANKHAAR J.-W., HOFMAN M. B., MARCUS J. T., ZWANENBURG J. J., FAES T. J., VONK-NOORDEGRAAF A.: Correction of phase offset errors in main pulmonary artery flow quantification. *J. Magn. Reson. Im. 22*, 1 (2005), 73–79. 2

[Loe63] LOEVE M.: *Probability Theory*, 3rd. ed. D. Van Nostrand, 1963. 2

[LTMG13] LIU W., TANG X., MA Y., GAO J.-H.: 3D phase unwrapping using global expected phase as a reference: Application to MRI global shimming. *Magn. Reson. Med. 70*, 1 (2013), 160–168. 2

[Lum67] LUMLEY J. L.: The structure of inhomogeneous turbulent flows. *Atmospheric turbulence and radio wave propagation* (1967), 166–178. 2

[MCC*13] MANJÓN J. V., COUPÉ P., CONCHA L., BUADES A., COLLINS D. L., ROBLES M.: Diffusion Weighted Image Denoising Using Overcomplete Local PCA, 2013. 2

[MFK*12] MARKL M., FRYDRYCHOWICZ A., KOZERKE S., HOPE M., WIEBEN O.: 4D Flow MRI. *J. Magn. Reson. Im. 36*, 5 (2012), 1015–1036. 2

[MHB*07] MARKL M., HARLOFF A., BLEY T. A., ZAITSEV M., JUNG B., WEIGANG E., LANGER M., HENNIG J., FRYDRYCHOWICZ A.: Time-resolved 3D MR velocity mapping at 3T: Improved navigator-gated assessment of vascular anatomy and blood flow. *J. Magn. Reson. 25*, 4 (2007), 824–831. 3

[MKS*97] MCCONNELL M., KHASGIWALA V., SAVORD B., CHEN M., CHUANG M., EDELMAN R., MANNING W.: Comparison of respiratory suppression methods and navigator locations for MR coronary angiography. *Am. J. Roentgenol. 168*, 5 (1997), 1369–75. 2

[MSS*08] MCGREGOR R., SZCZERBA D., SIEBENTHAL M., MURALIDHAR K., SZÉKELY G.: Exploring the Use of Proper Orthogonal Decomposition for Enhancing Blood Flow Images Via Computational Fluid Dynamics. In *Medical Image Computing and Computer-Assisted Intervention – MICCAI 2008*. Springer, 2008, pp. 782–789. 2

[PTA*11] POBITZER A., TUTKUN M., ANDREASSEN O., FUCHS R., PEIKERT R., HAUSER H.: Energy-scale aware feature extraction for unsteady flow visualization. *Comp. Graph. Forum 30*, 3 (2011). 2, 3

[RE06] RICHTER Y., EDELMAN E. R.: Cardiology is flow. *Circulation 113*, 23 (2006), 2679–2682. 1

[SFH*10] STALDER A. F., FRYDRYCHOWICZ A., HARLOFF A., YANG Q., BOCK J., HENNIG J., LI K. C., MARKL M.: Vortex Core Detection and Visualization using 4D Flow-sensitive MRI. In *Proc. Intl. Soc. Mag. Reson. Med.* (2010), vol. 18, p. 3708. 1

[SGSM08] SALZBRUNN T., GARTH C., SCHEUERMANN G., MEYER J.: Pathline predicates and unsteady flow structures. *The Visual Computer 24*, 12 (2008), 1039–1051. 2

[Sir87] SIROVICH L.: Turbulence and the dynamics of coherent structures. *Q. Appl. Math. 45* (1987), 561–571. 2

[vPOBB*10] VAN PELT R., OLIVAN BESCOS J., BREEUWER M., CLOUGH R. E., GRÖLLER E., TER HAAR ROMENIJ B., VILANOVA A.: Exploration of 4D MRI Blood Flow using Stylistic Visualization. *IEEE Trans. Vis. Comput. Graph. 16*, 6 (2010), 1339–1347. 2

[WFR*10] WASER J., FUCHS R., RIBIČIĆ H., SCHINDLER B., BLÖSCHL G., GRÖLLER E.: World Lines. *IEEE Trans. Vis. Comput. Graph. 16*, 6 (2010), 1458–1467. 3

[WKM08] WEISHAUPT D., KÖCHLI V. D., MARINCEK B.: *How Does MRI Work?* Springer, 2008. 2